Simulation Performance of 55 Imaging Air-Cherenkov Telescopes HAWC's Eye at High Altitude

J. Serna-Franco,[a,*] **R. Alfaro,**[a] **J. Audehm,**[b] **T. Bretz,**[b] **O. Chaparro-Amaro,**[c] **G. Do,**[b] **M.M. González,**[d] **F. González,**[d] **A. Iriarte,**[d] **J. Martínez-Castro,**[c] **M. Martínez-Felipe,**[c] **F. Maslowski,**[b] **Y. Pérez,**[d] **F. Rehbein,**[b] **F. Tischbein,**[b] **I. Torres**[e] **and M. Schaufel**[f]

[a]*Instituto de Física, Universidad Nacional Autónoma de México, Mexico*

[b]*Physics Institute III A, RWTH Aachen University, Germany*

[c]*Centro de Investigación en Computación, Instituto Politécnico Nacional, Mexico*

[d]*Instituto de Astronomía, Universidad Nacional Autónoma de México, Mexico*

[e]*Instituto Nacional de Astrofísica, Óptica y Electrónica, Mexico*

[f]*Physics Institute III B, RWTH Aachen University, Germany*

  E-mail: j_serna@ciencias.unam.mx

Preliminary results from the analysis of first data from hybrid observation campaigns using a compact light-weight Imaging Air-Cherenkov Telescope (IACT), named *HAWC's Eye*, and the *High-Altitude Water Cherenkov* (*HAWC*) observatory have shown that some features of the air-shower detection in HAWC, as the angular resolution, could be enhanced. Therefore an array of such devices could be an interesting upgrade for modern and future experiments such as the HAWC Observatory or the *Southern Wide-field Gamma-ray Observatory* (*SWGO*). In this work, the results of simulated observations of extensive air-showers by the array of 55 HAWC's Eye IACTs, are shown. An extensive library of simulated primary particles as γ-rays and protons in an energy range from 1 TeV to 100 TeV at an altitude of 4,100 m a.s.l. was produced. The features and performance of such an array are discussed in this work.

*37*th *International Cosmic Ray Conference (ICRC 2021)*
July 12th – 23rd, 2021
Online – Berlin, Germany

---

*Presenter

1. Introduction

The Universe has too many unsolved questions and mysteries to be discovered. The models used to describe and understand these phenomena are limited due to our knowledge. For this reason, the discovery of cosmic rays started a new era for theoretical models and marked the beginning of new and more sophisticated detection techniques. *Imaging Air-Cherenkov Telescopes* (IACTs) utilize a common technique for the detection of γ-rays by observing Cherenkov radiation emitted by extensive air-showers induced when interacting with the Earth's atmosphere. Simultaneous stereoscopic observations with an array of telescopes generally improves the overall performance. An array of compact telescopes with a lower energy threshold around 10 TeV was suggested as an extension for the High Altitude Water Cherenkov Observatory [1] and as a veto for the IceCube observatory [2].

This work presents preliminary results from the analysis of a simulation of an array of 55 such compact and light-weighted telescopes called *HAWC's Eye*.

2. The Imaging Air-Cherenkov Telescope HAWC's Eye

The *HAWC's Eye* telescope is a compact and light-weight imaging air-Cherenkov telescope [3] that has already been tested at the *High-Altitude Water Cherenkov* (*HAWC*) observatory [4], and a preliminary cosmic-ray spectrum has been obtained [5].

The telescope has a 549.7 mm Fresnel lens on top to focus the light on the camera located in the focal plane at a distance of 502.1 mm from the lens. The camera is composed of 64 Semiconductor Photo Multipliers (SiPMs) of type MicroFJ-60035-TSV (ON Semiconductor, previously SensL), where 61 of the SiPM-based pixels are equipped with a solid light guide made from Polymethyl Methacrylate (PMMA) to increase their effective light-collection area. The first camera of this type was commissioned in the *First G-APD Cherenkov Telescope* (*FACT*) in 2011 [6]. The other three pixels without light guides, called blind pixels, are used for monitoring purposes. The active pixels have a field-of-view of 1.5° each, yielding a total field-of-view of 12°. The sensors are located inside a 3D-printed case mounted on the camera's printed circuit board to protect the pixels from damage. A carbon barrel protects the camera from environmental effects and supports the Fresnel lens as well.

The Data Acquisition (DAQ) system is an adaptation of the DAQ used in the FACT telescope, and it is composed of a pre-amplifier, a trigger-unit, and an analog-to-digital converter [6]. The whole electronics is placed inside a water-tight carbon-fiber box. For the trigger, the camera is divided into six patches of nine and one patch of seven pixels. The signals in each patch are summed and compared with pre-defined thresholds. Only events for which at least one patch exceeds the threshold are recorded. The signals are sampled by the Domino Ring Sampling 4 (DRS4 [7]) chips with a sampling rate of 2 GS/s. Figure 1 depicts some parts of the HAWC's Eye telescope previously mentioned. A more detailed description can be found in [3].

In particular, their low price of roughly 10,000 Euro per telescope makes them an interesting option for an extension of existing detectors such as HAWC, or the future *Southern Wide-field Gamma-ray Observatory* (*SWGO*) [8].
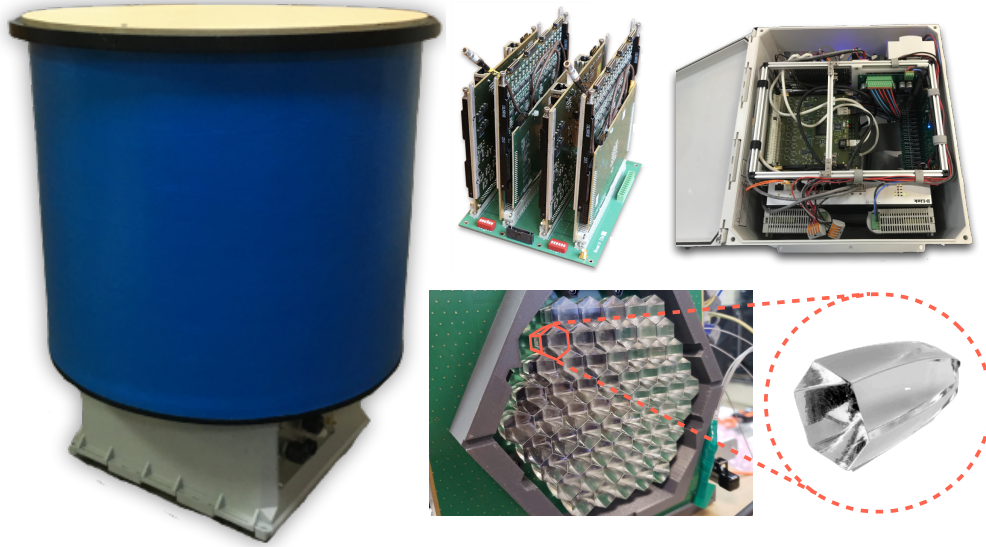
Figure 1: Left: The HAWC's Eye telescope assembled. The telescope's blue light-tight barrel with a wood cover that protects the Fresnel lens from external stress. Upper-right: the DAQ boards provided by the FACT collaboration, and the complete DAQ system placed inside its protective shield. Bottom-right: the 64-pixel camera. Each pixel is composed by a SiPM sensor of type SenseL MicroFJ, and a hex-to-square solid light guide made of PMMA.

3. The HAWC's Eye Array

To assess the performance of an array of telescopes, 55 HAWC's Eye telescopes have been simulated with an equally-spaced mutual distance of 20 m. Figure 2 shows the layout. To account for the anticipated hybrid detection, characteristics of the HAWC observatory were considered. The HAWC observatory is an extensive air-shower detector located in Sierra Negra, Mexico, with an altitude of 4,100 m a.s.l., and it is constituted by 300 Water Cherenkov Detectors (WCD) which cover an area of 22,000 m^2 [9]. For simulations of the telescope array, the covered area, elevation, and atmosphere model were used, matching the HAWC environment.

Inside the array, a few telescopes are located in non-regular places. Matching the coordinate system of the simulated array with the HAWC detector, the locations correspond to positions at which real telescopes were placed during previous observation campaigns [10, 11].

Extensive air-showers were simulated with CORSIKA V7.69 contemplating γ-rays and protons as the primary particles with energies between 1 TeV and 100 TeV and an integral spectral index of -1.5. So far, more than three million simulated events have been produced for each species. Further details on the configuration setup used can be found in [12].

For the detector simulation and image reconstruction, the MARS analysis software[13] has been used. For energy reconstruction, a Random Forest [14] based package, *ranger* [15], was applied.
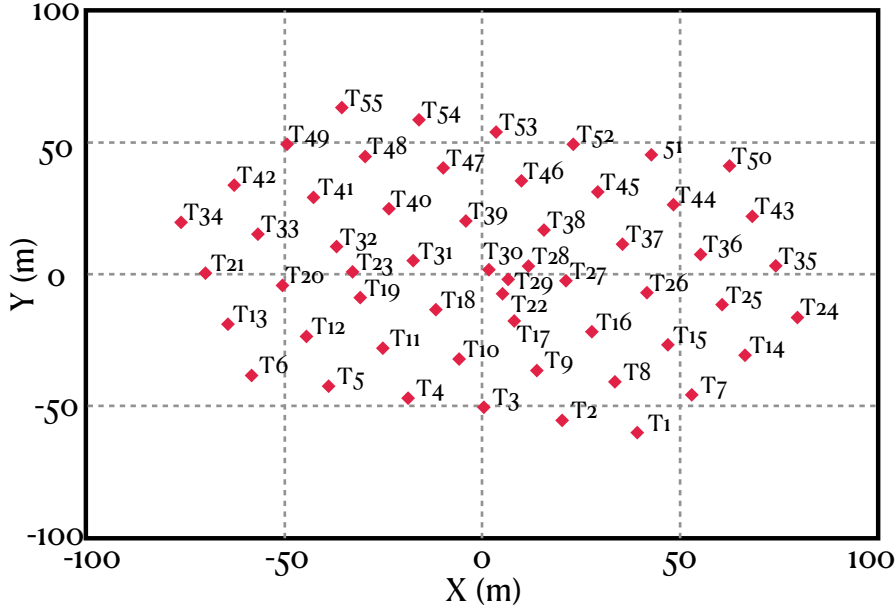
Figure 2: The 55 HAWC's Eye telescopes array. All the telescopes have an equally-spaced mutual distance along the covered area, but four are at special locations where telescopes were placed during observation campaigns previously performed (telescopes 22, 23, 28, and 29).

4. Simulation Training

The total sample of simulated events has been divided into two subsets. One subset is used to train (70%) the method and the other one for the analysis (30%). The Random Forest has been trained for regression of $\log_{10}(E)$ for each telescope and each particle species individually based on a list of ten image parameters that were obtained from the cleaned, i. e. background free, image. These are: *'Alpha', 'Dist', 'Lenght', 'Width'*: the so-called Hillas parameters describing orientation, location and shape of the image, *'log10SizeMainIsland'*: logarithm of the sum of the signals of the brightest cluster of pixels, *'log10size'*: logarithm of the total signal of the image, *'Leakage1'*: fraction of the signal in the outermost pixel ring of the camera, *'TimeSpread'*: spread of the arrival times of all image signals, *'TimeSpreadWeighted'*: spread of the arrival times weighted with the pixel signal. In addition, the simulated *'Impact'* position of the primary particle relative to the telescope's position smeared with a two-dimensional Gaussian distribution with a width of $\sigma = 4$m has been included. The width of the distribution corresponds to the average resolution of the HAWC detector.

As the telescopes were simulated independently, the image parameter distribution of each telescope should be independent of the telescope position. Figure 3 compares the distribution of the calculated second moments of the light distribution (Width and Length) for all the telescopes in the array. In both cases, no significant deviation between individual telescopes is visible.
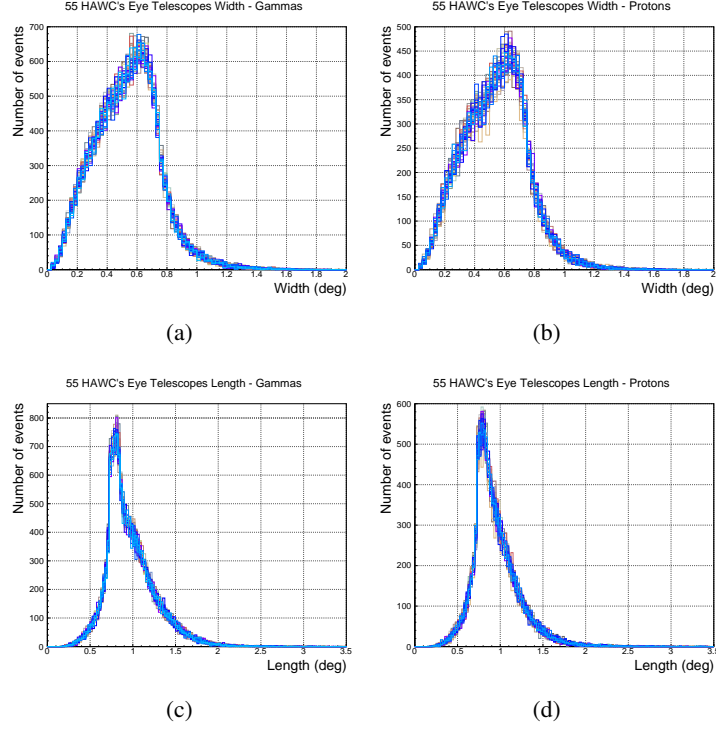
Figure 3: Distribution of the width parameter for (*a*) γ-rays events and (*b*) proton events, The distribution of the length parameter for (*c*) γ-rays events and (*d*) proton events; for the 55 HAWC's Eye telescopes in the array. No significant deviation between telescopes is visible as expected.

5. HAWC's Eye Telescopes Array Performance

The energy is an essential parameter of the array that must be analyzed to test its performance. Here, results for γ-rays and protons are presented.

After the image cleaning and reconstruction process, about 25 thousand events remain. Figure 4 shows the correlation between the reconstructed energy (E_{Reco}) and the Monte Carlo energy (E_{MC}) for both species, exemplary for three random telescopes (6, 25, and 30). A good correlation is visible. As expected from shower physics, the resolution for γ-rays is slightly better. At the lowest and highest energies, an unavoidable reconstruction bias is visible due to the cut-off of the distribution by the energy threshold and the limitation of the simulated energy range.

6. Energy resolution

From the predicted energy (E_{MC}) and the true energy (E_{MC}), the energy resolution,

$$\frac{1}{\sqrt{N}}\sqrt{\sum_{i=1}^{N}\left[\log_{10}(E_{\text{Pred},i}) - \log_{10}(E_{\text{MC},i})\right]^2},$$

was computed for each telescope, and their average. The energy resolution for proton events is shown in Figure 5(a), and for γ-ray events in Figure 5(b). At low and high energies, a systematic bias due to the discussed edge effects is visible.

5

7. Angular resolution

For the prediction of the arrival direction the Random Forest was trained considering the center-of-gravity of the light distribution, *'Leakage2'*: The fraction of signal in the two outermost pixel rings, the third moment along the major axis M3Long, Leakage1, and the smeared impact position as described above (Section 4). As the Random Forest does not handle cyclic variables well, two forests were trained to predict the Cartesian coordinates $(x, y) = (\theta\cos(\phi)), \theta\sin(\phi))$ independently, with θ and ϕ being the zenith and azimuth angle of the primary's arrival direction. As an estimation for the angular resolution, the mean value of the angular distance $\Delta = \cos^{-1}(\vec{r}_{\text{True}} \cdot \vec{r}_{\text{Pred}})$ was chosen between the normalized simulated arrival direction $\vec{r}_{\text{True}}$ and the normalized predicted direction $\vec{r}_{\text{Pred}}$.

The resulting resolution for protons (a) and gammas (b) is shown in Figure 6 for each of the 55 telescopes in the array together with their average.

Again, edge effects below the energy threshold and at the limit of the simulated energy range are visible. For both protons and gammas the quoted mean angular deviation corresponds roughly to the 60% containment, while the 50% containment lies a factor of 0.8 lower and the 90% containment a factor of 1.9 higher.
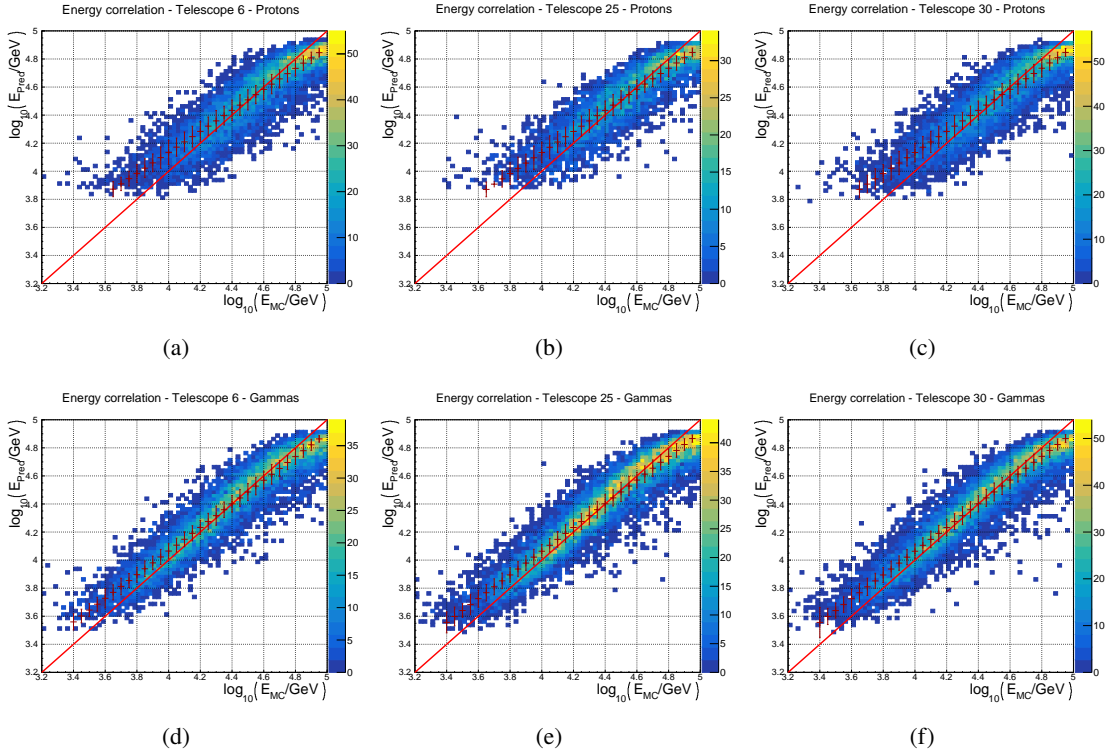

Figure 4: Energy correlation for three representative telescopes of the array depicted for a slope of -1.5. (*a*) Telescope 6 with protons events. (*b*) Telescope 25 with protons events. (*c*) Telescope 30 with protons events. (*d*) Telescope 6 with γ-ray events. (*e*) telescope 25 with γ-ray events. (*f*) Telescope 30 with γ-ray events. The peak of the distribution towards high energies originates from the flat simulated spectrum with a slope of only -1.5. The red error bars correspond to the RMS value of the distribution in each energy bin.
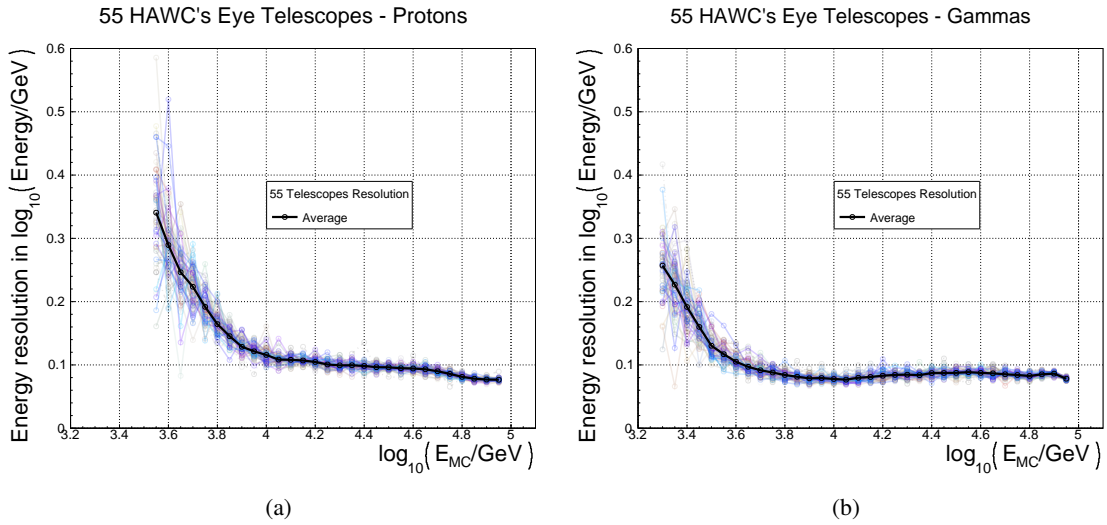
Figure 5: Energy resolution as a function of the Monte Carlo energy. The colored lines depict the resolution for each of the 55 telescopes for (*a*) γ-ray events and (*b*) proton events. The average resolution of the telescopes is shown in a solid black line.
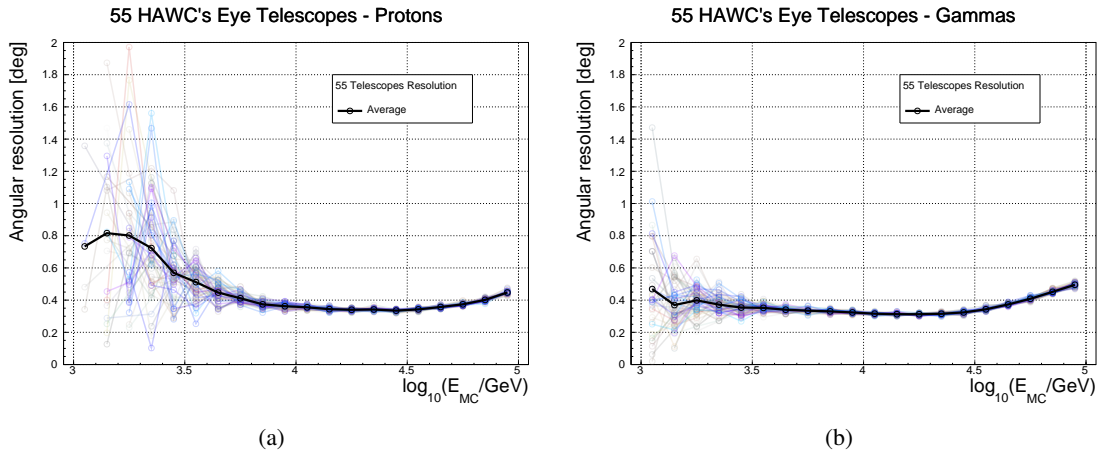

Figure 6: Angular resolution as a function of the Monte Carlo energy. The colored lines depict the resolution for each of the 55 telescopes for (*a*) γ-ray events and (*b*) proton events. The average resolution of the telescopes is shown in a solid black line.

8. Summary and Outlook

A 55 HAWC's Eye telescopes array was simulated, considering the environment of the HAWC observatory and the typical core resolution of a densely spaces extensive air-shower array. A database of three million γ-rays and protons each was built for an energy range of 1 TeV to 100 TeV. First results on the performance of the array were obtained. An improvement in energy and angular resolution was obtained even in a hybrid configuration with monoscopic telescope observations. As expected, results are independent of the telescope position. Further improvements in stereo configuration have been shown previously and will be studied in details in the future, which makes

7

an array of compact imaging air-Cherenkov telescopes a promising application as an upgrade for extensive air-shower arrays such as the HAWC observatory, and the *South Wide-field Gamma-ray Observatory* (*SWGO*).

9. Acknowledgements

References

[1] Schaufel, M., et al. (2018, August). In 35th International Cosmic Ray Conference (Vol. 301, p. 786). SISSA Medialab.

[2] Rysewyk, D. et al. (2020). Astroparticle Physics, 117, 102417.

[3] Bretz, T. et al. (2018). Journal of instrumentation, 13(07), P07024.

[4] Audehm, J. et al. (2019). In 36th International Cosmic Ray Conference (ICRC2019) (Vol. 36, p. 636).

[5] Rehbein, F. et al. (2021). In 37th International Cosmic Ray Conference. PoS(2021)397.

[6] Anderhub, H. et al. (2013). Journal of Instrumentation, 8(06), P06008.

[7] Ritt, S. (2008). In 2008 IEEE Nuclear Science Symposium Conference Record (pp. 1512-1515). IEEE.

[8] Assis, P. et al. (2018). Astroparticle Physics, 99, 34-42.

[9] Abeysekara, A. U. et al. (2017). The Astrophysical Journal, 843(1), 39.

[10] Audehm, J. (2020). Master's thesis, RWTH-Aachen, Aachen, Germany.

[11] Do, G. (2021). Master's thesis, RWTH-Aachen, Aachen, Germany.

[12] Rehbein, F. et al. (2021). In International Cosmic Ray Conference. PoS(ICRC2021)397.

[13] Bretz, T. et al. (2003). In International Cosmic Ray Conference (Vol. 5, p. 2947).

[14] Albert, J. et al. (2008). Nuclear Instruments and Methods in Physics Research Section A: Accelerators, Spectrometers, Detectors and Associated Equipment, 588(3), 424-432.

[15] Wright, M. N., & Ziegler, A. (2015). arXiv preprint arXiv:1508.04409.